



Transition Bimetal Based MOF Nanosheets for Robust Aqueous Zn Battery

Jun Wan^{1,2}, Junfeng Li^{1,2}, Zhiheng Xiao¹, Dandan Tang³, Bo Wang^{4*}, Yongjun Xiao^{5*} and Weilin Xu^{1*}

¹ State Key Laboratory for Hubei New Textile Materials and Advanced Processing Technology, Wuhan Textile University, Wuhan, China, ² Hubei Key Laboratory of Biomass Fiber and Ecological Dyeing and Finishing, School of Chemistry and Chemical Engineering, Wuhan Textile University, Wuhan, China, ³ Institute of China Rural Studies, Central China Normal University, Wuhan, China, ⁴ School of Electrical Engineering and Automation, Luoyang Institute of Science and Technology, Luoyang, China, ⁵ School of Physics and Electronic Information Engineering, Hubei Engineering University, Xiaogan, China

OPEN ACCESS

Edited by:

Liang Huang,
Huazhong University of Science and
Technology, China

Reviewed by:

Teng Zhai,
Nanjing University of Science and
Technology, China
Fengjuan Chen,
Lanzhou University, China

*Correspondence:

Bo Wang
bowang@lit.edu.cn
Yongjun Xiao
xiaoyj2016@hust.edu.cn
Weilin Xu
weilin_xu@hotmail.com

Specialty section:

This article was submitted to
Energy Materials,
a section of the journal
Frontiers in Materials

Received: 27 April 2020

Accepted: 25 May 2020

Published: 24 June 2020

Citation:

Wan J, Li J, Xiao Z, Tang D, Wang B,
Xiao Y and Xu W (2020) Transition
Bimetal Based MOF Nanosheets for
Robust Aqueous Zn Battery.
Front. Mater. 7:194.
doi: 10.3389/fmats.2020.00194

High-performance, good stability, low-cost, and environmentally friendly batteries are important for multifunctional electronics and electric vehicles. Compared with the high-energy density lithium-ion batteries, aqueous rechargeable battery has been extensively researched due to high safety, low cost and much better rate performance. Here, we report a one-step approach to fabricate porous Ni-Cu metal-organic framework (MOF) nanosheet arrays structures for stable energy storage with a high-energy (71.2 mWh cm⁻³) and high-stability (capacity retention of ≈91% after 2,500 cycles) performance. Furthermore, we synthesized various porous homogeneous Ni-Co, Ni-Zn, Ni-Fe and Ni-Mn bimetal MOF structures with high surface area and conductivity utilizing this rational design. This work provides a simple efficient strategy for constructing porous homogeneous bimetal MOF nanosheet arrays with high energy and stability performance, holding a great potential for future portable electronics.

Keywords: bimetal, metal organic framework, nanosheet, high-stability, Zn battery

INTRODUCTION

With the ever-increasing demand for renewable energy sources and conversion techniques, energy storage devices with high energy and power densities, good reliability, and long cycling life are urgently required (Bonaccorso et al., 2015; Wan et al., 2016; Zhai et al., 2018). Although high-energy density lithium-ion batteries have been extensively researched, the overall performance and wide usage have been limited due to their relatively low power density and safety (Kim et al., 2013; Li J. et al., 2015; Xu et al., 2019). By contrast, aqueous rechargeable battery is of particular interest owing to high safety, low cost, and much better rate performance (Duan et al., 2016; Gao et al., 2018; Stock et al., 2019). Zinc-based batteries are an alternative energy source due to their high theoretic capacity (819 mAhg⁻¹), relatively low redox potential and extensive global reserves (Pan et al., 2016; Fu et al., 2019). Particularly, compared with the output voltage of other aqueous batteries (mostly ≤1.2 V), nickel-zinc (Ni-Zn) battery has a higher output voltage (≈1.8 V) (Huang et al., 2013; Wang R. et al., 2018). However, the formation of zinc dendrite at anode and irreversible reactions at cathode during the electrochemical reaction will lead to inferior discharge performance and poor cycling stability (<500 cycles) (Liu et al., 2016). Therefore, designing good functionally and structurally stable electrode nanomaterials with high-activity nanostructures is highly important.

Metal-organic frameworks, as porous crystalline coordination polymers, which are formed by coordination bonds between metal atom nodes and organic ligands with periodic structural units (Yaghi and Li, 1995). Due to the highly porous structural characteristics, MOFs could provide a larger exposure reaction surface for fast ion/mass transport, resulting in a high capacitance and rate capability performance (Wu et al., 2017; Qiu et al., 2018). For instance, Dennis et al. first utilizing high electrical conductive MOFs ($\text{Ni}_3(\text{HITP})_2$) for supercapacitors without other binders (Sheberla et al., 2016). Choi et al. prepared and examined 23 different structure nMOFs with multiple organic functionalities and metal ions, which exhibit exceptionally high capacitance (Choi et al., 2014). However, MOFs still have the issue of bad stability, poor conductivity and the blocking of active sites by organic ligands (Li et al., 1999). Recently, two kinds of metallic elements have been incorporated in the crystallization process to successfully synthesize the homogeneous bimetallic MOF topology with different molar ratios (Yan et al., 2017; Wang X.L. et al., 2018). It's electrochemical properties and stability can be significantly improved due to the synergistic interactions, such as improved charge transfer between dopants and host metal atoms (Huang et al., 2018; Wang H. et al., 2018). For example, Li et al. synthesized a mesoporous $\text{Ni}_{0.3}\text{Co}_{2.7}\text{O}_4$ nanorod derived by Co/Ni-MOFs, which delivered a large reversible capacity of $1,410 \text{ mAhg}^{-1}$ after 200 cycles at a current of 100 mA g^{-1} with an high-rate capability for lithium-ion batteries (Li et al., 2016). Yan et al. reported a Ni-Co bimetal phosphide $\text{Ni}_{0.6}\text{Co}_{1.4}\text{P}$ nanocages as highly efficient electrocatalysts with long-term stability (10 h for continuous test) via phosphorization from $\text{Ni}_{0.6}\text{Co}_{1.4}(\text{OH})_2$ metal-organic framework (Qiu et al., 2018). Additionally, as unique 2D nanostructures could exhibit rapid ion/mass transport, high specific surface area and high percentages of exposed active coordinative metal sites, it would be of great significance to develop 2D MOFs and derived arrayed structures (Zhao et al., 2016; Wu et al., 2020). Thus, combining the homogeneous bimetallic MOF topology and 2D arrayed nanostructures would offer an ideal model to construct highly efficient electrode material with long-term stability and explore precise structure-performance relationships at atomic/molecular levels (Dang et al., 2017; Wan et al., 2017).

Herein, we presented a novel one-step approach to synthesize various porous bimetal organic framework nanosheet arrays structures for stable energy storage. Through mixing solvents, benzenedicarboxylic acid (BDC), nickel foam and different bimetallic precursors and maintained at 130°C for 2 h, we successfully synthesized porous homogeneous Ni-Co, Ni-Cu, Ni-Zn, Ni-Fe and Ni-Mn bimetal MOFs (expressed as Ni,Co-MOF, Ni,Cu-MOF, Ni,Zn-MOF, Ni,Fe-MOF and Ni,Mn-MOF). The as-synthesized nickel foams are uniformly coated with 2D arrayed porous bimetal MOFs, resulting in a high surface area and conductive current collector. Additionally, benefiting from the uniform distribution of metal centers, the Ni-Cu bimetal MOF achieves a high-energy (71.2 mWh cm^{-3}) performance and high-stability (capacity retention of $\approx 91\%$ after 2500 cycles) assembling into a battery. This work provides a simple efficient strategy for constructing robust cathode materials of Ni-Zn

battery, which may pave the way for the rational design of high energy storage technology.

MATERIALS AND METHODS

Materials

Benzenedicarboxylic acid (BDC) was obtained from Shanghai Aladdin Bio-Chem Technology Co., Ltd., and all other chemicals were purchased from Sinopharm Chemical Reagent Co., Ltd. All the solvents used in this study were of analytical grades.

Synthesis of Ni-MOF

First, 30 ml ethanol and 2 ml deionization water were mixed in a 50 ml Teflon-liner. Then 0.3 mmol BDC and 0.3 mmol $\text{Ni}(\text{NO}_3)_2 \cdot 6\text{H}_2\text{O}$ were added into the solution, while sonicated for about 30 min and put a nickel foam (2 2 cm) into the mixed solution. Finally, the 50 ml Teflon-lined autoclave was sealed and maintained at 130°C for 2 h. The product was washed by ethanol and deionization water.

Synthesis of Ni,Cu-MOF

After mixing 30 ml ethanol and 2 ml deionization water in a 50 ml Teflon-liner, the 0.3 mmol BDC, 0.15 mmol $\text{Ni}(\text{NO}_3)_2 \cdot 6\text{H}_2\text{O}$ and 0.15 mmol $\text{Cu}(\text{NO}_3)_2 \cdot 3\text{H}_2\text{O}$ were added into the mixed solution and sonicated for 30 min. With a nickel foam (2 2 cm) putting into the solution, the 50 ml Teflon-lined autoclave was maintained at 130°C for 2 h.

Synthesis of Other Bimetallic MOFs

The synthesis processes of Ni,Co-MOF, Ni,Zn-MOF, and Ni,Mn-MOF were same as the preparation of Ni,Cu-MOF, expect that 0.15 mmol $\text{Cu}(\text{NO}_3)_2 \cdot 3\text{H}_2\text{O}$ was replaced by 0.15 mmol $\text{Co}(\text{NO}_3)_2 \cdot 6\text{H}_2\text{O}$, $\text{Zn}(\text{NO}_3)_2 \cdot 6\text{H}_2\text{O}$ and $\text{Mn}(\text{NO}_3)_2 \cdot 4\text{H}_2\text{O}$, respectively. In the process of Ni,Fe-MOF, 0.24 mmol $\text{Ni}(\text{NO}_3)_2 \cdot 6\text{H}_2\text{O}$ and 0.06 mmol $\text{Fe}(\text{NO}_3)_3 \cdot 9\text{H}_2\text{O}$ were added into the mixed solution.

Electrical Measurements

For a typical three-electrode system, an Ag/AgCl reference electrode, an Pt plate counter electrode, and a Celgard separator (3501 Coated PP, Celgard LLC) were used in 1 M KOH aqueous solution. All tests were conducted in a three-neck Swagelok cells (t-branch pipe, Swagelok). They were pressed between two stainless steel rods from two necks of the Swagelok cells, and a third neck was used to put a reference electrode into the cell. Cyclic voltammograms (CVs), galvanostatic charge/discharge and impedance spectroscopy were performed by an electrochemical workstation (CHI 760E). The capacitance (C) values were calculated by the equation $C = \int (IV)/(m\nu\Delta V)$. The electrochemical characterizations of all full batteries were tested in a two-electrode cell in a solution of 1 M KOH and 0.02 M $\text{Zn}(\text{Ac})_2$. The anode is a zinc plate with a thickness of 0.15 mm.

Characterization

The morphology size, crystal structure of samples were determined by the scanning electron microscopy (SEM, FEI Nova 450 Nano), transmission electron microscopy (TEM, TECNAI G2 20 U-TWIN), XPS (AXISULTRA DLD-600W)

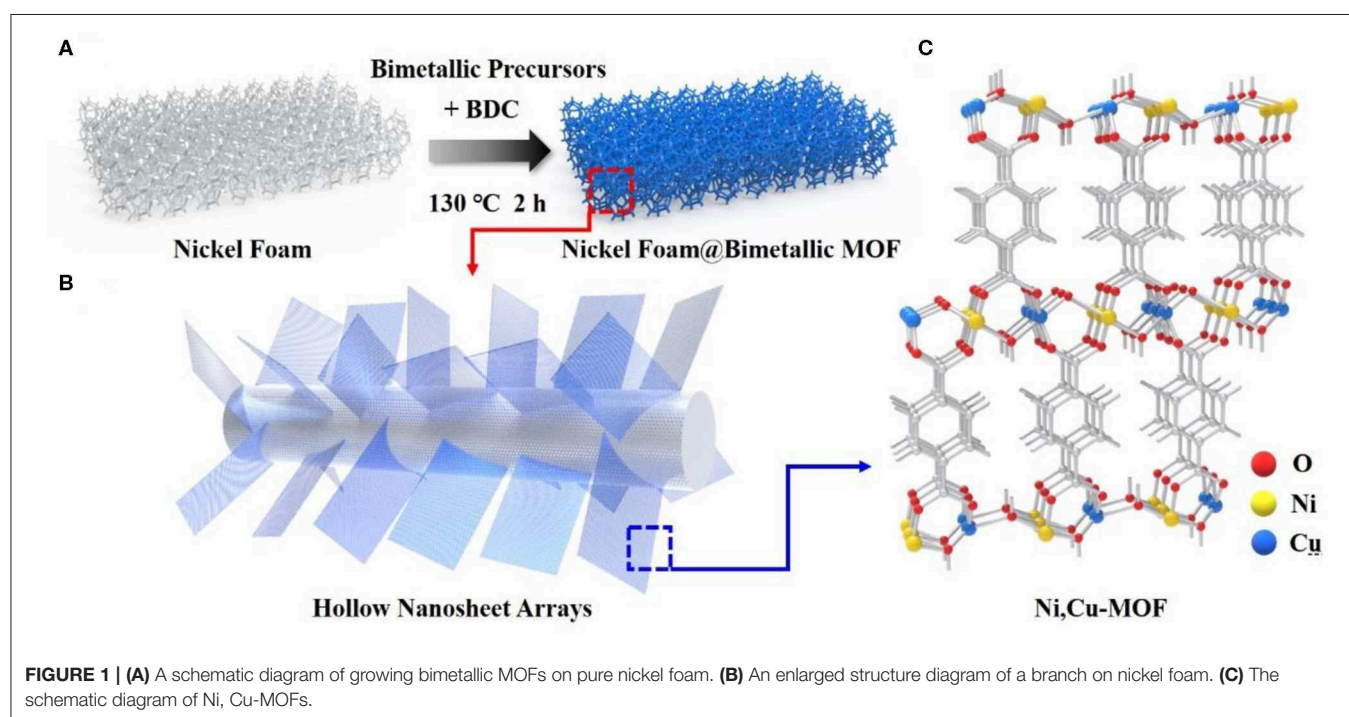
and X-ray diffraction using Cu-K α radiation ($\lambda = 1.5418 \text{ \AA}$) (XRD, Philips X' Pert Pro). The mass loading was measured using a microbalance (CPA225D, Sartorius). All electrochemical performance were performed by the ECLab and CHI660E instruments.

RESULTS AND DISCUSSION

The synthetic strategy for the various porous bimetal-organic framework nanosheet arrays is schematically depicted in **Figure 1**. Briefly, the BDC and different bimetallic precursors were added into ethanol and deionization water, then a nickel foam was put into the solution with sonicating for about 30 min. After reacting at 130°C for 2 h in a 50 ml Teflon-lined autoclave, Ni derived MOF and various Ni-Co, Ni-Cu, Ni-Zn, Ni-Fe, and Ni-Mn bimetal MOFs were gradually formed by coordination bonds between metal atom nodes and organic ligands with periodic structural units (Zhao et al., 2016). In this bimetallic MOF structure, six O atoms co-formed the octahedron of Ni and Cu atoms. Four of the six O atoms from carboxylates or hydroxyls and two of them form the other one. Then, the octahedral structure will be connected in the direction of [010] on the (200) lattice plane in the form of edges/angles, finally forming a two-dimensional bimetallic layer separated by BDC molecules. The corresponding bimetallic precursors including $\text{Ni}(\text{NO}_3)_2 \cdot 6\text{H}_2\text{O}$, $\text{Co}(\text{NO}_3)_2 \cdot 6\text{H}_2\text{O}$, $\text{Cu}(\text{NO}_3)_2 \cdot 3\text{H}_2\text{O}$, $\text{Zn}(\text{NO}_3)_2 \cdot 6\text{H}_2\text{O}$, $\text{Mn}(\text{NO}_3)_2 \cdot 4\text{H}_2\text{O}$, and $\text{Fe}(\text{NO}_3)_3 \cdot 9\text{H}_2\text{O}$. Meanwhile, the hydrolysis controlled ion exchange and etching process ($\text{Ni}^{2+} + 2\text{H}_2\text{O} = \text{Ni}(\text{OH})_2 + 2\text{H}^+$, where the H^+ will etch the MOF to create central void space) contribute to the germination of highly porous 2D arrays nanostructure (Guan et al., 2017).

Subsequently, we characterize the morphological and compositional features of the Ni,Cu-MOF sample with scanning electron microscopy (SEM) and transmission electron microscopy (TEM). The Ni,Cu-MOF sample after reaction becomes blue, which suggests that a metathesis between the Cu^{2+} cations and the Ni^{2+} cations in the MOF framework and a coating on nickel foam (**Figure S1**). As shown in **Figures 2a,b**, the nanosheet arrays are uniformly coated on nickel foam with a large area. The TEM image of the powder further indicates the porous structures on nanosheets (**Figure 2c**). It corresponds to the Brunauer–Emmett–Teller (BET) surface areas of $178.87 \text{ m}^2 \text{ g}^{-1}$ (**Figure S2**). In order to observe the distribution of different elements, the Energy-dispersive X-ray spectroscopy (EDS) elemental mapping was conducted (**Figure 2d**). The corresponding mapping images show the homogeneous distribution of Ni and Cu. The mole ratio of Ni:Cu is about 1.5, which is further confirmed by the inductively coupled plasma mass spectrometry (ICP-MS). These results indicate the successful preparation of Ni,Cu-MOF. Additionally, we may readily control the composition of the resulting porous bimetal organic framework nanostructures. Following a similar process, Ni-Co, Ni-Zn, Ni-Fe and Ni-Mn bimetal MOFs were gradually formed, which were all nanosheet arrays uniformly coated on nickel foams (**Figure S3**).

To explore the crystal structure and surface states of products, we applied the X-ray diffraction (XRD), X-ray photoelectron spectroscopy (XPS) and Raman analyses. **Figure 3A** shows all XRD patterns for Ni-MOF, Ni,Co-MOF, Ni,Cu-MOF, Ni,Zn-MOF, Ni,Fe-MOF, and Ni,Mn-MOF samples, revealing that the products are isostructural to the previously reported Ni-based MOFs (No. 985792) (Mesbah et al., 2014; Zhao et al., 2016).



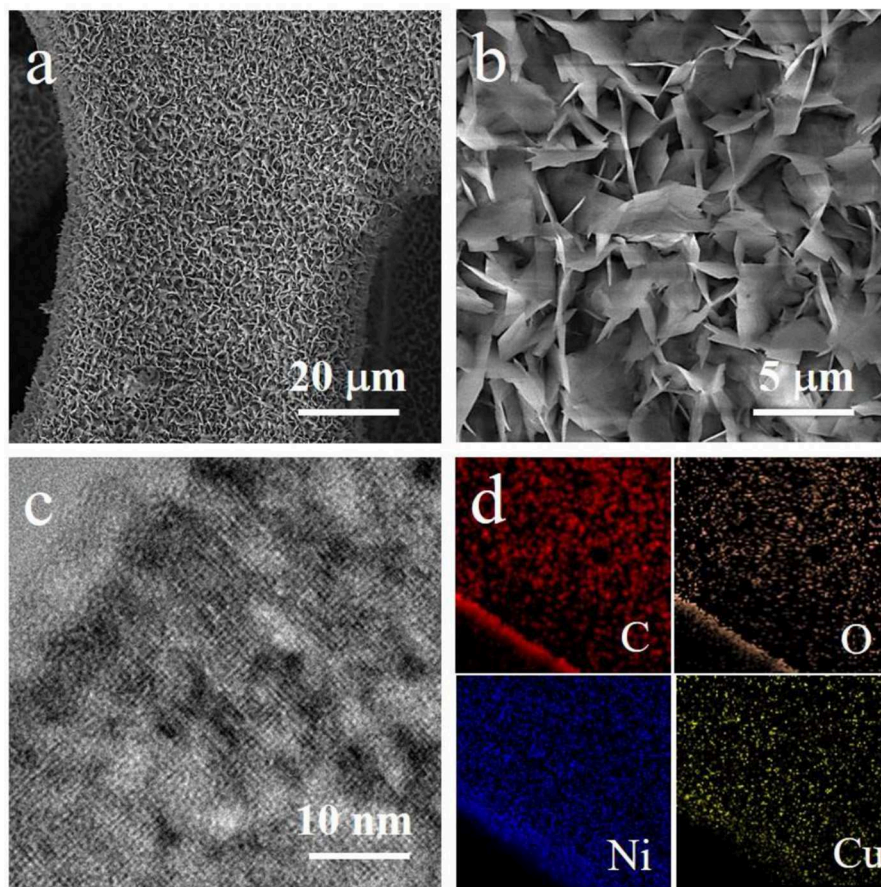


FIGURE 2 | SEM images of (a,b) Ni,Cu-MOF coated nickel foam. (c) TEM image of the porous Ni,Cu-MOF nanosheet. (d) EDS elemental mapping scanning from TEM for the corresponding nanosheet.

As shown in the magnification of the XRD patterns, the 2θ value of the (200) diffraction peaks clearly shift toward smaller diffraction angles with an increase in the lattice size (Figure S4). This phenomenon may result from the larger atom radius of Co (1.16 Å), Cu (1.17 Å), Zn (1.25 Å), Fe (1.17 Å), Mn (1.17 Å) than that of Ni (1.15 Å). Meanwhile, the lattice size of Ni,Zn-MOF has the largest change, which is matched with the biggest atomic radius. Furthermore, with the introduction of Cu element, the diffraction peaks of the Ni,Cu-MOF are still identical to the Ni-MOF, suggesting the Cu^{2+} partly substituted for Ni^{2+} in the metal-organic frameworks could retain the Ni-MOF crystal structure (Brozek and Dincă, 2013; Sun et al., 2015). In addition, XPS is used to probe the surface chemical valence. The survey spectrum of Ni,Cu-MOF shows the coexistence of Ni, Cu, O and C atoms with an elemental composition of Ni:Cu close to 1.46 (oxygen may be caused by the exposure of product in the air) (Figure S5), matching well with the ICP-MS result discussed above. Compared with the common Ni^0 peaks at 853 eV and 870 eV of nickel foam (Figure S6) (Wang R. et al., 2018), the additional characteristic Ni^{2+} , Ni^{3+} peaks and two shakeup satellites of Ni,Cu-MOF are fitted with two spin-orbit doublets and confirm the successful formation of

nickel oxides upon the reaction process (Figure 3B) (Yuan et al., 2012). It can be seen that the Ni^{2+} peaks shift to a higher binding energy compared to Ni-MOF, indicating that partial electrons transfer from Ni^{2+} to Cu^{2+} . The addition of copper can enhance the valence state of nickel, and the higher valence state of Ni (referred to as Ni^*) atoms have a strong ability to accept electrons, which corresponds to the previous reports (Burke et al., 2015; Zhao et al., 2016; Li et al., 2017). The peaks centered at 935.2 and 955.7 eV can be assigned to the Cu $2p_{3/2}$ and Cu $2p_{1/2}$ (Figure 3C). Additionally, the typical core level O 1s XPS spectra of the Ni,Cu-MOF is displayed in Figure 3D. The peak at 529.6 eV is typical metal-oxygen bonds, and the peaks at 531.3 and 531.8 eV correspond to the defects with surface oxygen and adsorbed water, respectively (Guan et al., 2017). In addition to verifying this bimetal strategy is applicable to the preparation of other metal organic frameworks, we following synthesize different bimetal MOFs including Ni,Co-MOF, Ni,Zn-MOF, Ni,Fe-MOF, and Ni,Mn-MOF.

Based on the uniform 2D arrayed porous bimetal organic framework nanostructures, it can not only provide high surface area, good electrical conductivity and short ion diffusion length, but also ensure high active site, making it a very

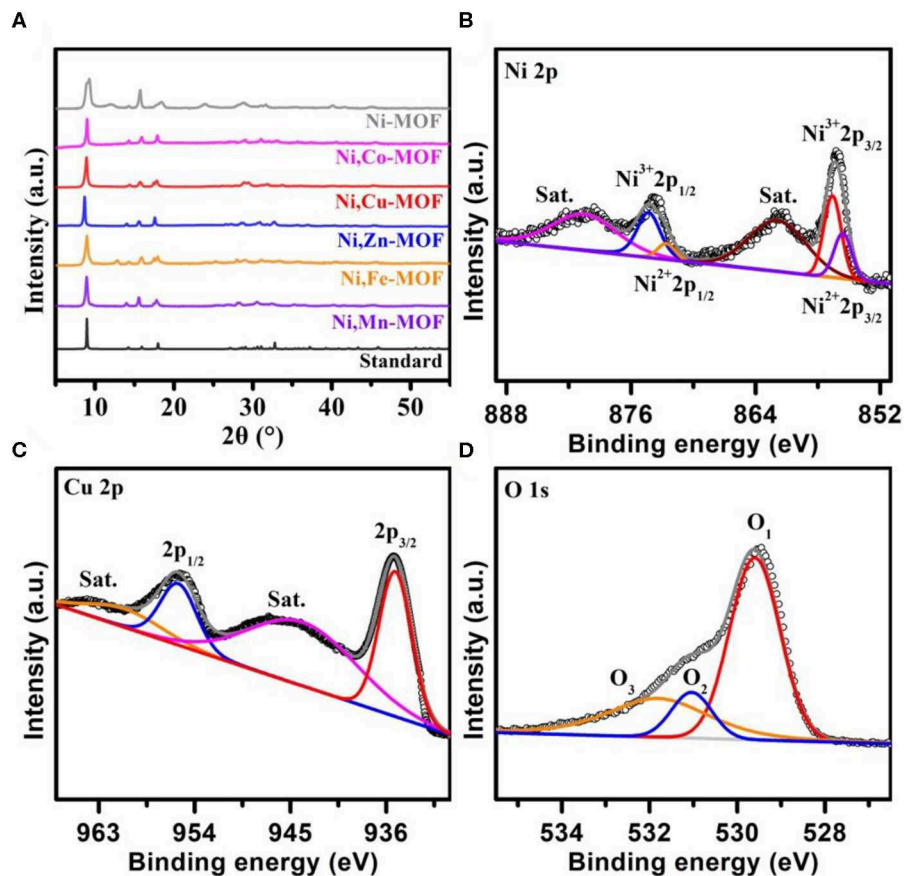


FIGURE 3 | (A) The XRD patterns of Ni-MOF, Ni,Co-MOF, Ni,Cu-MOF, Ni,Zn-MOF, Ni,Fe-MOF, Ni,Mn-MOF and the standard pattern, respectively. **(B–D)** High-resolution XPS spectra of Ni 2p, Cu 2p, and O 1s.

promising electrode material for energy storage applications. The electrochemical properties of nickel foam, Ni-MOF, Ni,Cu-MOF, Ni,Co-MOF, Ni,Zn-MOF, Ni,Fe-MOF and Ni,Mn-MOF electrodes were firstly tested in a three-electrode system using a 1 M KOH aqueous solution as the electrolyte, a Pt plate as the counter electrode, and a Ag/AgCl as the reference electrode. As shown in the cyclic voltammograms (CV) curves in the potential range from 0 to 0.6 V at a same scan rate of 10 mV s^{-1} , in addition to the nickel foam has little performance (**Figure S7**), others all exhibit obvious redox reactions between Ni^{2+} and Ni^{3+} with OH^- (**Figure 4A**) (Guan et al., 2016). It can be seen that the bimetal MOF electrodes exhibited much higher current density than that of the Ni-MOF electrode, indicating that the capacity can be greatly improved by homogeneous bimetal hybridity. **Figure 4B** comparatively shows the typical charge and discharge curves of all samples at 2 mA cm^{-2} , where all curves show characteristic charge and discharge plateaus at $0.25 \text{ V} \sim 0.35 \text{ V}$ and $0.3 \text{ V} \sim 0.35 \text{ V}$, respectively. The smallest difference value of the charging and discharging platforms of Ni,Cu-MOF indicates the least polarization and good reversibility, which is conducive to its cyclic stability (**Figure S8**). Conversely, the values of Ni,Zn-MOF and Ni,Mn-MOF are relatively large and resulting

in their poor cyclic stability. Impressively, Ni,Cu-MOF and Ni,Zn-MOF all reach a remarkable high capacity of 1.8 and 2.0 C cm^{-2} at 0.5 mA cm^{-2} (**Figure 4C**). When the current density increased from 1 to 80 mA cm^{-2} , the Ni,Cu-MOF electrode could retain a capacity of 53.0%, indicating that the Ni-Cu bimetal based cathode had a good rate capability. Compared with valuable areal capacity due to the support of nickel foam, specific capacity evaluated by mass loading is also important. As shown in **Figure S9**, the Ni,Cu-MOF and Ni,Zn-MOF show the maximum specific capacity of 1,837 and $2,086 \text{ C g}^{-1}$ at 0.5 A g^{-1} . All details of CV curves at different scan rates and GCD curves at different current density of Ni-MOF, Ni,Co-MOF, Ni,Cu-MOF, Ni,Zn-MOF, Ni,Fe-MOF, Ni,Mn-MOF samples are shown in **Figures S10–S15**. Additionally, cycling stability is another one of the key parameters of batteries. The Ni,Zn-MOF electrode shows a drastic capacity decay of 70% over 1,500 cycles, while the Ni,Cu-MOF electrode shows a gradual increase at the beginning and an overall decay of 6% over 5000 cycles (**Figure 4D**). In order to explain this phenomenon, the electrode of Ni,Zn-MOF after reaction was characterized by SEM in **Figure S16**. The electrode structure is no longer a porous nanosheet arrays, and the collapsed structure directly affects the

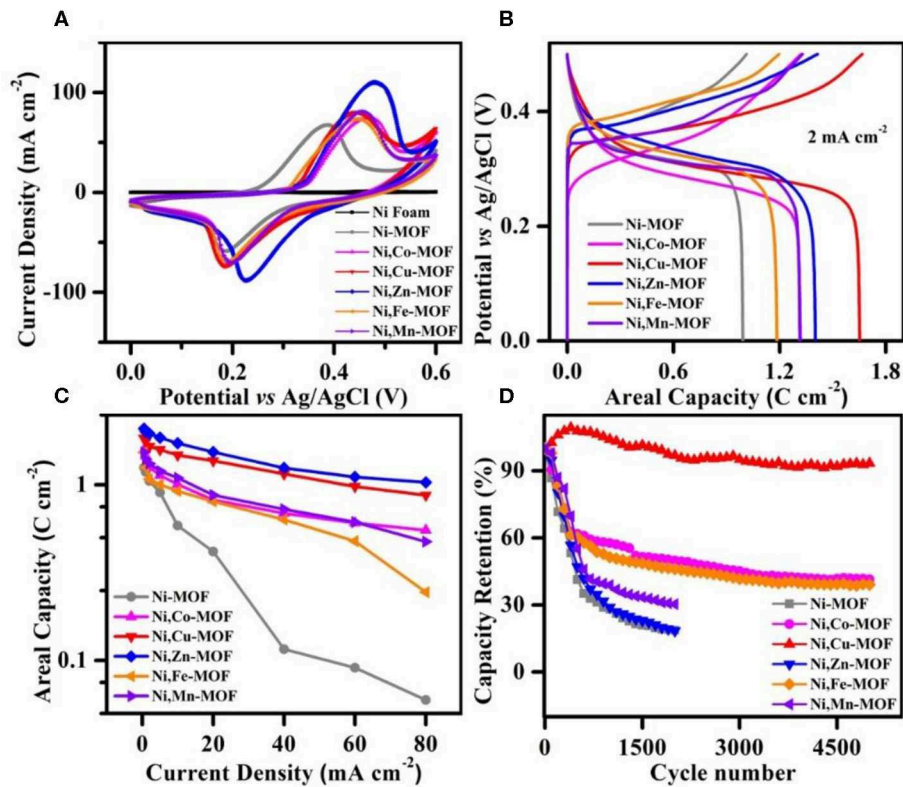


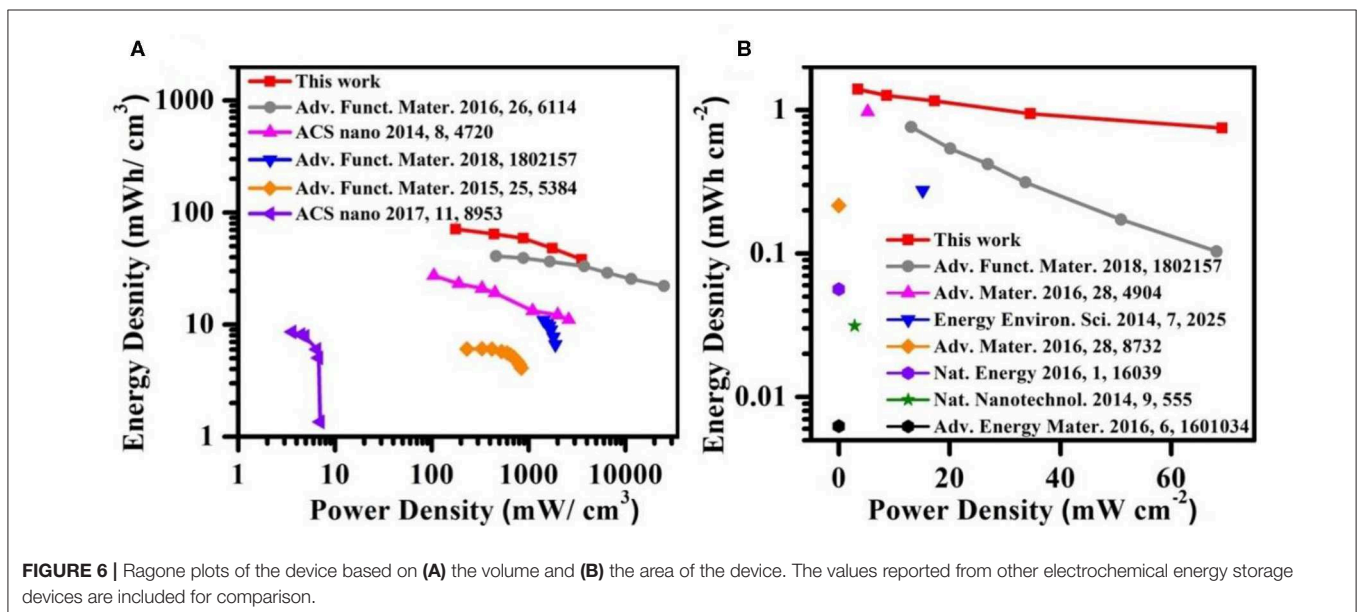
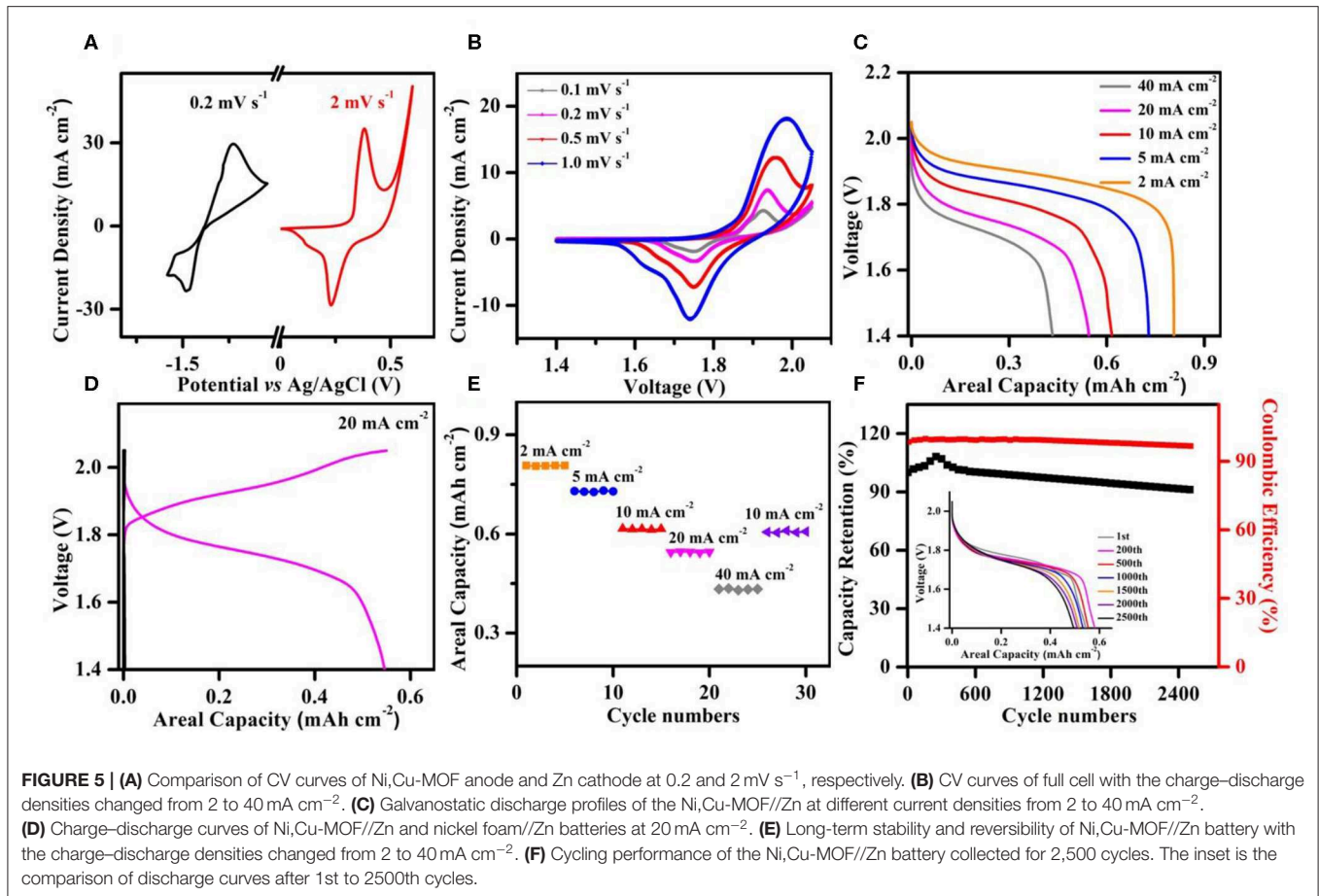
FIGURE 4 | (A) CV curves of the Ni foam, Ni-MOF, Ni,Co-MOF, Ni,Cu-MOF, Ni,Zn-MOF, Ni,Fe-MOF, and Ni,Mn-MOF, respectively. (B) Charge-discharge curves at 2 mA cm^{-2} . (C) Rate performance of all samples. (D) Cycling performance collected for 2,500 cycles.

cycling stability. Additionally, the increase in capacity during the initial cycling stage is likely due to activation of the active materials (Kim et al., 2015). The SEM images of other electrodes after cycling test showed that the hierarchical structure were well maintained, which further confirming the excellent cycling behavior (Figure S17). Compared with the poor cycling stability of Ni-MOF, these results suggest that bimetal strategy is benefit to the stability of metal organic frameworks for batteries.

To further probe the application of the robust Ni,Cu-MOF anode material, a full cell was assembled with a commercial Zn plate as cathode material (denoted as Ni,Cu-MOF//Zn). Figure 5A shows the CV curves of the Zn plate and Ni,Cu-MOF electrodes at 0.2 and 2 mV s^{-1} in 1 M KOH and 0.02 M Zn(Ac)_2 electrolyte, where both electrodes are composed of a pair of strong redox peaks. Consequently, the full cell was assembled and two typical CV curves were displayed in Figure 5B. A pair of reduction and oxidation peaks were observed at ≈ 1.75 and $\approx 1.95 \text{ V}$, respectively. The representative galvanostatic discharge (GD) curves of the full cell collected at different current densities were illustrated in Figure 5C, revealing its superior electrochemical performance with a discharge plateau at $\approx 1.7 \text{ V}$ with negligible voltage hysteresis even under 40 mA cm^{-2} . Moreover, the typical voltage-capacity curves of the Ni,Cu-MOF//Zn battery and Ni foam//Zn battery at 20 mA cm^{-2} were presented in Figure 5D. As expected, the Ni,Cu-MOF//Zn battery discharge plateau was longer and the capacity

of $0.55 \text{ mA h cm}^{-2}$ was higher. The coulombic efficiency of the Ni,Cu-MOF//Zn battery was 99.3%, demonstrating that the electrochemical property was improved obviously. The high-rate performance of the Ni,Cu-MOF//Zn battery was further evaluated in Figure 5E. The obtained cell showed a stable high-rate characteristic, and the capacities were ranging from $0.807 \text{ mA h cm}^{-2}$ at 2 mA cm^{-2} to $0.432 \text{ mA h cm}^{-2}$ at 40 mA cm^{-2} . When the current density was suddenly recovered to 10 mA cm^{-2} after 30 cycles, the average capacity of this battery could be restored to $0.607 \text{ mA h cm}^{-2}$, proving its good electrochemical reversibility. One of the main bottlenecks of aqueous rechargeable batteries is the inferior cycle stability. Based on the rapid ion/mass transport by porous 2D arrays and highly reversible redox behavior by bimetal incorporation, the Ni,Cu-MOF//Zn battery could still retain 92% of its original capacity after 2500 cycles and the coulombic efficiency during charging/discharging process was close to 99% (Figure 5F). The discharge curves of the Ni,Cu-MOF//Zn battery compared with the original profile after cycling for 2500th were shown in the inset of Figure 5F. The little attenuation of capacity clarified the good compressibility and a great promise for energy storage devices.

The energy density and power density are two important parameters for describing electrochemical performance of Ni,Cu-MOF//Zn battery (Wu et al., 2019; Liu et al., 2020). As revealed in Figure 6A, the as-fabricated Ni,Cu-MOF//Zn



battery exhibited a maximum voluminal energy density of 71.23 mWh cm⁻³ at a power density of 3530.61 mW cm⁻³, which outperforms most reported asymmetric supercapacitors and

aqueous electrolyte-based batteries, such as hVCNT2//hVCNT2 (41 mWh cm⁻³) (Wu et al., 2016), FGN-300//FGN-300 (27.2 mWh cm⁻³) (Yan et al., 2014), SANF//Zn (15.1 mWh cm⁻³)

(Wang R. et al., 2018), CNTs//Fe₃O₄-C (1.56 mWh cm⁻³) (Li R. et al., 2015), NiCo//Zn (8 mWh cm⁻³) (Huang et al., 2017). Additionally, the areal energy density of 1.40 mWh cm⁻² at a power density of 59.2 mW cm⁻² is also consistently high when compared with other researchs like SANF//Zn (0.754 mWh cm⁻²) (Wang R. et al., 2018), Zn//Co₃O₄ (0.97 mWh cm⁻²) (Wang et al., 2016), NiAlCo LDH/CNT//Zn (0.27 mWh cm⁻²) (Gong et al., 2014), CC-CF@NiO//CC-CF@ZnO (0.22 mWh cm⁻²) (Liu et al., 2016), Zn//MnO₂ (0.06 mWh cm⁻²) (Pan et al., 2016), SWNT/rGO//SWNT/rGO (0.03 mWh cm⁻²) (Yu et al., 2014) and CF@NiO//CF@Fe₃O₄ (0.006 mWh cm⁻²) (Guan et al., 2016) (Figure 6B).

CONCLUSION

In conclusion, a new one-step approach to fabricate porous bimetal organic framework nanosheet arrays nanostructures were successfully applied for stable energy storage. Due to the synergetic effect of bimetal incorporation and 2D arrayed nanostructures topology, the charge transfer between the dopants and the host metal atoms and rapid ion/mass transport can significantly enhance the electrochemical properties and stability. For aqueous recharge-able Ni-Zn battery applications, the outstanding performance of Ni,Cu-MOF//Zn battery which achieved a maximum energy density of 71.23 mWh cm⁻³ (1.40 mWh cm⁻²) and a maximum power density of 3,530.61 mW cm⁻³ (59.2 mW cm⁻²) in 1 M KOH electrolyte indicates the importance of homogeneous bimetallic MOF topology. Remarkably, the Ni,Cu-MOF//Zn could provide promising cycling durability with about 92% capacity retention after 2,500 cycles. This bimetal organic frameworks derived strategy may open up new opportunities for the rational design of homogeneous porous nanostructures and stable energy storage device.

REFERENCES

- Bonaccorso, F., Colombo, L., Yu, G., Stoller, M., Tozzini, V., Ferrari, A. C., et al. (2015). Graphene, related two-dimensional crystals, and hybrid systems for energy conversion and storage. *Science* 347:1246501. doi: 10.1126/science.1246501
- Brozek, C. K., and Dincă, M. (2013). Ti³⁺-, V^{2+/3+}-, Cr^{2+/3+}-, Mn²⁺-, and Fe²⁺-substituted MOF-5 and redox reactivity in Cr- and Fe-MOF-5. *J. Am. Chem. Soc.* 135, 12886–12891. doi: 10.1021/ja4064475
- Burke, M. S., Kast, M. G., Trotochaud, L., Smith, A. M., and Boettcher, S. W. (2015). Cobalt-iron (O_x) hydroxide oxygen evolution electrocatalysts: the role of structure and composition on activity, stability, and mechanism. *J. Am. Chem. Soc.* 137, 3638–3648. doi: 10.1021/jacs.5b00281
- Choi, K. M., Jeong, H. M., Park, J. H., Zhang, Y. B., Kang, J. K., and Yaghi, O. M. (2014). Supercapacitors of nanocrystalline metal-organic frameworks. *ACS Nano* 8, 7451–7457. doi: 10.1021/nn5027092
- Dang, S., Zhu, Q. L., and Xu, Q. (2017). Nanomaterials derived from metal-organic frameworks. *Nat. Rev. Mater.* 3:17075. doi: 10.1038/natrevmats.2017.75
- Duan, B., Gao, X., Yao, X., Fang, Y., Huang, L., Zhou, J., et al. (2016). Unique elastic N-doped carbon nanofibrous microspheres with hierarchical porosity derived

DATA AVAILABILITY STATEMENT

The raw data supporting the conclusions of this article will be made available by the authors, without undue reservation.

AUTHOR CONTRIBUTIONS

JW conceived the study designed the experiments, performed the experiments work, and wrote the manuscript. WX and BW perfected the revision of the manuscript. JL, ZX, and DT performed the SEM and TEM testing. YX analyzed the structure data. All authors approved the manuscript for publication. All authors contributed to the article and approved the submitted version.

FUNDING

This work was financially supported by the National Natural Science Foundation of China (51773158, 61971211), the Program for Youth Scholar Teachers Supporting Plan in Universities of Henan Province (2018GGJS157), the National Project Cultivation Plan (193137), and the Hubei Key Laboratory of Biomass Fiber and Ecological Dyeing and Finishing Open Fund (184083027).

ACKNOWLEDGMENTS

The authors thank to the facility support of the State Key Laboratory for Hubei New Textile Materials and Advanced Processing Technology and the Analysis and Testing Center of Wuhan Textile University.

SUPPLEMENTARY MATERIAL

The Supplementary Material for this article can be found online at: <https://www.frontiersin.org/articles/10.3389/fmats.2020.00194/full#supplementary-material>

from renewable chitin for high rate supercapacitors. *Nano Energy* 27, 482–491. doi: 10.1016/j.nanoen.2016.07.034

Fu, J., Liang, R., Liu, G., Yu, A., Bai, Z., Yang, L., et al. (2019). Recent progress in electrically rechargeable zinc-air batteries. *Adv. Mater.* 31:1805230. doi: 10.1002/adma.201805230

Gao, L., Xiong, L., Xu, D., Cai, J., Huang, L., Zhou, J., et al. (2018). Distinctive construction of chitin-derived hierarchically porous carbon microspheres/polyaniline for high-rate supercapacitors. *ACS Appl. Mater. Interfaces* 10, 28918–28927. doi: 10.1021/acsami.8b05891

Gong, M., Li, Y., Zhang, H., Zhang, B., Zhou, W., Feng, J., et al. (2014). Ultrafast high-capacity NiZn battery with NiAlCo-layered double hydroxide. *Energy Environ. Sci.* 7, 2025–2032. doi: 10.1039/c4ee00317a

Guan, C., Liu, X., Ren, W., Li, X., Cheng, C., and Wang, J. (2017). Rational design of metal-organic framework derived hollow NiCo₂O₄ arrays for flexible supercapacitor and electrocatalysis. *Adv. Energy Mater.* 7:1602391. doi: 10.1002/aenm.201602391

Guan, C., Zhao, W., Hu, Y., Ke, Q., Li, X., Zhang, H., et al. (2016). High-performance flexible solid-state Ni/Fe battery consisting of metal oxides coated carbon cloth/carbon nanofiber electrodes. *Adv. Energy Mater.* 6:1601034. doi: 10.1002/aenm.201601034

- Huang, L., Chen, D., Ding, Y., Wang, Z. L., Zeng, Z., and Liu, M. (2013). Hybrid composite Ni(OH)₂@NiCo₂O₄ grown on carbon fiber paper for high-performance supercapacitors. *ACS Appl. Mater. Interfaces* 5, 11159–11162. doi: 10.1021/am403367u
- Huang, L., Yao, X., Yuan, L., Yao, B., Gao, X., Wan, J., et al. (2018). 4-butylbenzenesulfonate modified polypyrrole paper for supercapacitor with exceptional cycling stability. *Energy Storage Mater.* 12, 191–196. doi: 10.1016/j.ensm.2017.12.016
- Huang, Y., Ip, W. S., Lau, Y. Y., Sun, J., Zeng, J., Yeung, N. S. S., et al. (2017). Weavable, conductive yarn-based NiCo//Zn textile battery with high energy density and rate capability. *ACS Nano* 11, 8953–8961. doi: 10.1021/acsnano.7b03322
- Kim, H., Jeong, G., Kim, Y. U., Kim, J. H., Park, C. M., and Sohn, H. J. (2013). Metallic anodes for next generation secondary batteries. *Chem. Soc. Rev.* 42, 9011–9034. doi: 10.1039/c3cs60177c
- Kim, S. K., Kim, H. J., Lee, J. C., Braun, P. V., and Park, H. S. (2015). Extremely durable, flexible supercapacitors with greatly improved performance at high temperatures. *ACS Nano* 9, 8569–8577. doi: 10.1021/acsnano.5b03732
- Li, H., Eddaoudi, M., O’Keeffe, M., and Yaghi, O. M. (1999). Design and synthesis of an exceptionally stable and highly porous metal-organic framework. *Nature* 402, 276–279. doi: 10.1038/46248
- Li, H., Liang, M., Sun, W., and Wang, Y. (2016). Bimetal-organic framework: one-step homogenous formation and its derived mesoporous ternary metal oxide nanorod for high-capacity, high-rate, and long-cycle-life lithium storage. *Adv. Funct. Mater.* 26, 1098–1103. doi: 10.1002/adfm.201504312
- Li, J., Liu, K., Gao, X., Yao, B., Huo, K., Cheng, Y., et al. (2015). Oxygen- and nitrogen-enriched 3D porous carbon for supercapacitors of high volumetric capacity. *ACS Appl. Mater. Interfaces* 7, 24622–24628. doi: 10.1021/acsmi.5b06698
- Li, N., Bediako, D. K., Hadt, R. G., Hayes, D., Kempa, T. J., von Cube, F., et al. (2017). Influence of iron doping on tetravalent nickel content in catalytic oxygen evolving films. *Proc. Natl. Acad. Sci. U.S.A.* 114, 1486–1491. doi: 10.1073/pnas.1620787114
- Li, R., Wang, Y., Zhou, C., Wang, C., Ba, X., Li, Y., et al. (2015). Carbon-stabilized high-capacity ferroferric oxide nanorod array for flexible solid-state alkaline battery-supercapacitor hybrid device with high environmental suitability. *Adv. Funct. Mater.* 25, 5384–5394. doi: 10.1002/adfm.201502265
- Liu, B., Sun, S., Jia, R., Zhang, H., Zhu, X., Zhang, C., et al. (2020). Oxygen-deficient homo-interface toward exciting boost of pseudocapacitance. *Adv. Funct. Mater.* 30:1909546. doi: 10.1002/adfm.201909546
- Liu, J., Guan, C., Zhou, C., Fan, Z., Ke, Q., Zhang, G., et al. (2016). A flexible quasi-solid-state nickel-zinc battery with high energy and power densities based on 3D electrode design. *Adv. Mater.* 28, 8732–8739. doi: 10.1002/adma.201603038
- Mesbah, A., Rabu, P., Sibille, R., Lebègue, S., Mazet, T., Malaman, B., et al. (2014). From hydrated Ni₃(OH)₂(C₈H₄O₄)₂(H₂O)₄ to anhydrous Ni₂(OH)₂(C₈H₄O₄): impact of structural transformations on magnetic properties. *Inorg. Chem.* 53, 872–881. doi: 10.1021/ic402106v
- Pan, H., Shao, Y., Yan, P., Cheng, Y., Han, K. S., Nie, Z., et al. (2016). Reversible aqueous zinc/manganese oxide energy storage from conversion reactions. *Nat. Energy* 1:16039. doi: 10.1038/nenergy.2016.39
- Qiu, B., Cai, L., Wang, Y., Lin, Z., Zuo, Y., Wang, M., et al. (2018). Fabrication of nickel-cobalt bimetal phosphide nanocages for enhanced oxygen evolution catalysis. *Adv. Funct. Mater.* 28:1706008. doi: 10.1002/adfm.201706008
- Sheberla, D., Bachman, J. C., Elias, J. S., Sun, C. J., Shao-Horn, Y., and Dincă, M. (2016). Conductive mof electrodes for stable supercapacitors with high areal capacitance. *Nat. Mater.* 16, 220–224. doi: 10.1038/nmat4766
- Stock, D., Dongmo, S., Janek, J., and Schröder, D. (2019). Benchmarking anode concepts: the future of electrically rechargeable zinc-air batteries. *ACS Energy Lett.* 4, 1287–1300. doi: 10.1021/acsenerylett.9b00510
- Sun, D., Sun, F., Deng, X., and Li, Z. (2015). Mixed-metal strategy on metal-organic frameworks (MOFs) for functionalities expansion: Co substitution induces aerobic oxidation of cyclohexene over inactive Ni-MOF-74. *Inorg. Chem.* 54, 8639–8643. doi: 10.1021/acs.inorgchem.5b01278
- Wan, J., Wu, J., Gao, X., Li, T., Hu, Z., Yu, H., et al. (2017). Structure confined porous Mo₂C for efficient hydrogen evolution. *Adv. Funct. Mater.* 27:1703933. doi: 10.1002/adfm.201703933
- Wan, J., Yao, X., Gao, X., Xiao, X., Li, T., Wu, J., et al. (2016). Microwave combustion for modification of transition metal oxides. *Adv. Funct. Mater.* 26, 7263–7270. doi: 10.1002/adfm.201603125
- Wang, H., Li, X., Lan, X., and Wang, T. (2018). Supported ultrafine nico bimetallic alloy nanoparticles derived from bimetal-organic frameworks: a highly active catalyst for furfuryl alcohol hydrogenation. *ACS Catal.* 8, 2121–2128. doi: 10.1021/acscatal.7b03795
- Wang, R., Han, Y., Wang, Z., Jiang, J., Tong, Y., and Lu, X. (2018). Nickel@nickel oxide core-shell electrode with significantly boosted reactivity for ultrahigh-energy and stable aqueous Ni-Zn battery. *Adv. Funct. Mater.* 28:1802157. doi: 10.1002/adfm.201802157
- Wang, X., Wang, F., Wang, L., Li, M., Wang, Y., Chen, B., et al. (2016). An aqueous rechargeable Zn//Co₃O₄ battery with high energy density and good cycling behavior. *Adv. Mater.* 28, 4904–4911. doi: 10.1002/adma.201505370
- Wang, X. L., Dong, L. Z., Qiao, M., Tang, Y. J., Liu, J., Li, Y., et al. (2018). Exploring the performance improvement of the oxygen evolution reaction in a stable bimetal-organic framework system. *Angew. Chem. Int. Ed.* 57, 9660–9664. doi: 10.1002/anie.201803587
- Wu, J., Gao, X., Yu, H., Ding, T., Yan, Y., Yao, B., et al. (2016). A scalable free-standing V₂O₅/CNT film electrode for supercapacitors with a wide operation voltage (1.6 v) in an aqueous electrolyte. *Adv. Funct. Mater.* 26, 6114–6120. doi: 10.1002/adfm.201601811
- Wu, J., Xiong, L., Zhao, B., Liu, M., and Huang, L. (2020). Densely populated single atom catalysts. *Small Methods* 4:1900540. doi: 10.1002/smtd.201900540
- Wu, J., Zhou, H., Li, Q., Chen, M., Wan, J., Zhang, N., et al. (2019). Densely populated isolated single Co-N site for efficient oxygen electrocatalysis. *Adv. Energy Mater.* 9:1900149. doi: 10.1002/aenm.201900149
- Wu, L. L., Wang, Z., Long, Y., Li, J., Liu, Y., Wang, Q. S., et al. (2017). Multishelled Ni_xCo_{3-x}O₄ hollow microspheres derived from bimetal-organic frameworks as anode materials for high-performance lithium-ion batteries. *Small* 13:1604270. doi: 10.1002/smll.201604270
- Xu, H., Peng, C., Yan, Y., Dong, F., Sun, H., Yang, J., et al. (2019). “All-in-one” integrated ultrathin SnS₂@3D multichannel carbon matrix power high-areal-capacity lithium battery anode. *Carbon Energy* 1, 276–288. doi: 10.1002/cey2.22
- Yaghi, O. M., and Li, H. (1995). Hydrothermal synthesis of a metal-organic framework containing large rectangular channels. *J. Am. Chem. Soc.* 117, 10401–10402. doi: 10.1021/ja00146a033
- Yan, J., Wang, Q., Wei, T., Jiang, L., Zhang, M., Jing, X., et al. (2014). Template-assisted low temperature synthesis of functionalized graphene for ultrahigh volumetric performance supercapacitors. *ACS Nano* 8, 4720–4729. doi: 10.1021/nn500497k
- Yan, L., Cao, L., Dai, P., Gu, X., Liu, D., Li, L., et al. (2017). Metal-organic frameworks derived nanotube of nickel-cobalt bimetal phosphides as highly efficient electrocatalysts for overall water splitting. *Adv. Funct. Mater.* 27:1703455. doi: 10.1002/adfm.201703455
- Yu, D., Goh, K., Wang, H., Wei, L., Jiang, W., Zhang, Q., et al. (2014). Scalable synthesis of hierarchically structured carbon nanotube-graphene fibres for capacitive energy storage. *Nat. Nanotech.* 9, 555–562. doi: 10.1038/nnano.2014.93
- Yuan, C., Li, J., Hou, L., Zhang, X., Shen, L., and Lou, X. W. (2012). Ultrathin mesoporous NiCo₂O₄ nanosheets supported on Ni foam as advanced electrodes for supercapacitors. *Adv. Funct. Mater.* 22, 4592–4597. doi: 10.1002/adfm.201200994
- Zhai, T., Sun, S., Liu, X., Liang, C., Wang, G., and Xia, H. (2018). Achieving insertion-like capacity at ultrahigh rate via tunable surface pseudocapacitance. *Adv. Mater.* 30:1706640. doi: 10.1002/adma.201706640
- Zhao, S., Wang, Y., Dong, J., He, C. T., Yin, H., An, P., et al. (2016). Ultrathin metal-organic framework nanosheets for electrocatalytic oxygen evolution. *Nat. Energy* 1:16184. doi: 10.1038/nenergy.2016.184

Conflict of Interest: The authors declare that the research was conducted in the absence of any commercial or financial relationships that could be construed as a potential conflict of interest.

Copyright © 2020 Wan, Li, Xiao, Tang, Wang, Xiao and Xu. This is an open-access article distributed under the terms of the Creative Commons Attribution License (CC BY). The use, distribution or reproduction in other forums is permitted, provided the original author(s) and the copyright owner(s) are credited and that the original publication in this journal is cited, in accordance with accepted academic practice. No use, distribution or reproduction is permitted which does not comply with these terms.